### Title
Full range polarization-sensitive Fourier domain optical coherence tomography




### Journal
Optics Express, 12(24)

### ISSN
1094-4087



### Authors
Zhang, Jun
Jung, Woonggyu
Nelson, J. Stuart
et al.



### Publication Date
2004

### DOI
10.1364/OPEX.12.006033

Peer reviewed

# Full range polarization-sensitive Fourier domain optical coherence tomography

**Jun Zhang, Woonggyu Jung, J. Stuart Nelson, Zhongping Chen**

*Beckman Laser Institute and the Center for Biomedical Engineering*
*University of California, Irvine, California 92612*
*junzhang@uci.edu*

**Abstract:** A swept source based polarization-sensitive Fourier domain optical coherence tomography (FDOCT) system was developed that can acquire the Stokes vectors, polarization diversity intensity and birefringence images in biological tissue by reconstruction of both the amplitude and phase terms of the interference signal. The Stokes vectors of the reflected and backscattered light from the sample were determined by processing the analytical complex fringe signals from two perpendicular polarization-detection channels. Conventional time domain OCT (TDOCT) and spectrometer based FDOCT systems are limited by the fact that the input polarization states are wavelength dependent. The swept source based FDOCT system overcomes this limitation and allows accurate setting of the input polarization states. From the Stokes vectors for two different input polarization states, the polarization diversity intensity and birefringence images were obtained.



**OCIS codes:** (170.4500) Optical coherence tomography; (070.2590) Fourier transforms; (230.5440) Polarization-sensitive devices; (260.1440) Birefringence

## References and links

1. D. Huang, E. A. Swanson, C. P. Lin, J. S. Schuman, W. G. Stinson, W. Chang, M. R. Hee, T. Flotte, K. Gregory, C. A. Puliafito, J. G. Fujimoto, "Optical coherence tomography," Science **254**, 1178-1181 (1991).
2. A. F. Fercher, C. K. Hitzenberger, G. Kamp, and S. Y. Elzaiat, "Measurement of intraocular distances by backscattering spectral interferometry," Opt. Commun. **117**, 43-48 (1995).
3. G. Hausler and M. W. Linduer, "Coherence radar and spectral radar-new tools for dermatological diagnosis," J. Biomed. Opt. **3**, 21-31 (1998).
4. R. A. Leitgeb, C. K. Hitzenberger, and A. F. Fercher, "Performance of fourier domain vs. time domain optical coherence tomography," Opt. Express **11**, 889-894 (2003). http://www.opticsexpress.org/abstract.cfm?URI=OPEX-11-8-889.
5. S. H. Yun, G. J. Tearney, J. F. de Boer, N. Iftimia, and B. E. Bouma, "High-speed optical frequency-domain imaging," Opt. Express **11**, 2953-2963 (2003). http://www.opticsexpress.org/abstract.cfm?URI=OPEX-11-22-2953
6. R. A. Leitgeb, M. Wojtkowski, A. Kowalczyk, C. K. Hitzenberger, M. Sticker, and A. F. Fercher, "Spectral measurement of absorption by spectroscopic frequency-domain optical coherence tomography," Opt. Lett. **25**, 820-822 (2000).
7. R. A. Leitgeb, L. Schmetterer, C. K. Hitzenberger, A. F. Fercher, F. Berisha, M. Wojtkowski, and T.Bajraszewski, "Real-time measurement of in vitro flow by Fourier-domain color Doppler optical coherence tomography," Opt. Lett. **29**, 171-173 (2004).
8. Y.Yasuno, S.Makita, Y.Sutoh, M.Itoh, and T.Yatagai, "Birefringence imaging of human skin by polarization-sensitive spectral interferometric optical coherence tomography," Opt. Lett. **27**, 1803-1805 (2002).
9. H. Ren, Z. Ding, Y. Zhao, J. Miao, J. S. Nelson, and Z. Chen, " Phase-resolved functional optical coherence tomography: simultaneous imaging of in situ tissue structure, blood flow velocity, standard deviation, birefringence, and Stokes vectors in human skin," Opt. Lett. **27**, 1702-1704 (2002).
10. C. E. Saxer, J. F. de Boer, B. H. Park, Y. Zhao, Z. Chen, J. S. Nelson, "High-speed fiber based polarization-sensitive optical coherence tomography of in vivo human skin," Opt. Lett. **25**, 1355-1357 (2000).
11. J. E. Roth, J. A. Kozak, S. Yazdanfar, A. M. Rollins, J. A. Izatt, "Simplified method for polarization sensitive optical coherence tomography," Opt. Lett. **26**, 1069-1071 (2001).

#5440 - $15.00 US Received 7 October 2004; revised 19 November 2004; accepted 19 November 2004

12. D. P. Dav, T. Akkin, T. E. Milner, "Polarization-maintaining fiber-based optical low coherence reflectometer for characterization and ranging of birefringence," Opt. Lett. **28**, 1775-1777 (2003).

## 1. Introduction

Optical coherence tomography (OCT) is a noninvasive, noncontact imaging modality that uses coherent gating to obtain high-resolution cross-sectional images of tissue microstructure [1]. Compared with conventional time domain OCT (TDOCT) which is based on a scanning optical delay line, Fourier domain OCT (FDOCT) can obtain higher sensitivity and imaging speed [2-5]. In addition to the morphological structural image, FDOCT can also provide functional information of tissue physiology such as absorption [6] and blood flow velocity [7]. Tissue birefringence is another important functional parameter which can be measured by FDOCT. A spectrometer based FDOCT system was reported which incorporated bulk polarizers and wave plates to control the polarization states used to determine birefringence of the sample [8]. However, accurate control of the polarization states is difficult especially in the case of broad bandwidth because the wave plates are wavelength dependent. In TDOCT systems, a phase-resolved approach was demonstrated to be an effective method for high speed acquisition of polarization information [9]. This approach can also be used in FDOCT system to reconstruct intensity and birefringence images by processing the complex signals from the sample under study. However, the obscure object structure and phase error due to the mirror image generated by the Fourier transform and the low frequency noises originating from the reflected terms from the reference mirror and sample compromise the reconstruction of complex fringe signals. In this paper, a swept source FDOCT system was developed that can obtain the Stokes vectors, polarization diversity intensity and birefringence images in biological tissue. Complete removal of the autocorrelation noise and mirror image using an EO phase modulator achieved the full range complex signal. The polarization states generated by a polarization modulator were controlled accurately by selecting an appropriate drive function. A phase-resolved signal processing method was adopted to acquire the multifunctional images by processing the analytical interference complex fringe signals derived from two perpendicular polarization detection channels.

## 2. Experimental setup and signal processing

A schematic diagram of the fiber based FDOCT system is shown in Fig. 1. A 1310 nm swept laser (Micron Optics) with a FWHM bandwidth of 85 nm and output power of 5 mW was operated at the sweeping rate of 500 Hz. The output light was polarized to $45^{\circ}$ with respect to the optical axis of the crystal in the polarization modulator (New Focus). The polarization modulator was driven by a two step drive function to generate a phase shift of zero and $\pi/2$ at 250 Hz. The corresponding two Stokes vectors of the output light are orthogonal in the Poincaré sphere so that the birefringence measurements are independent of the orientation of the optical axis in the sample. Subsequently, the light was split into reference and sample arms by a $2 \times 2$ coupler. In the reference arm, a polarizing EO phase modulator (JDS Uniphase) was used to generate a stable carrier frequency of 1 MHz for elimination of the mirror image and low frequency noise. The EO phase modulator was driven by a ramp waveform with 40 MHz sampling rate. To match dispersion caused by the EO phase modulator, an optical setup similar to a rapid scanning optical delay line with a stationary mirror was adopted which can compensate the group velocity dispersion. Calculations showed that the higher order dispersion can be neglected in our system. The reference power was attenuated by an adjustable neutral density attenuator for maximum sensitivity. 5% of the laser output was split and propagated through a 100 GHz fiber Fabry-Perot (FFP) interferometer (Micron Optics) to generate comb signals for dynamic calibration of the swept wavenumber function that is essential for rigorous conversion from time to wavenumber space. In the detection arm, the interfered beam was split into two polarization channels by a

#5440 - $15.00 US Received 7 October 2004; revised 19 November 2004; accepted 19 November 2004

polarization beam splitter (PBS). The fringe signals from the two polarization channels were detected by two photodetectors and then converted by a 12 bit data acquisition board sampling at 10 MHz.

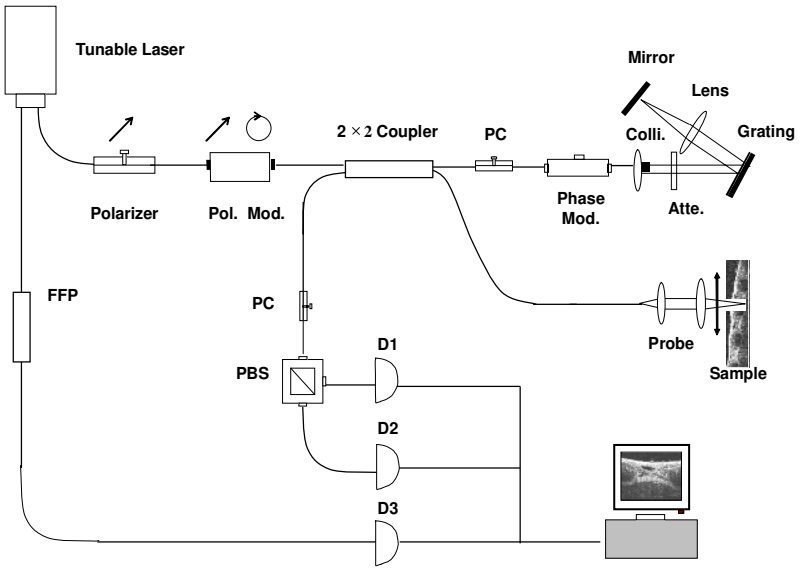


Fig. 1. Schematic of the FDOCT system. Pol. Mod.: polarization modulator; Phase Mod.: phase modulator; Colli.: collimator; Atte.: adjustable neutral density attenuator; FFP: 100 GHz fiber Fabry-Perot interferometer; PC: polarization controller; PBS: polarization beam splitter; D1, D2, D3: photodetectors.

The synchronizing time clock diagram of the system is shown in Fig. 2. Since the half wave voltage of the polarization modulator is proportional to the working wavelength, the phase shift and the corresponding polarization state would be wavelength dependent with a constant driven voltage. Assuming a Gaussian spectrum light source with the FWHM bandwidth of $\Delta\lambda$ and center wavelength $\lambda_0$, an average polychromatic phase error of $\Delta\phi = \phi_0 \Delta\lambda / (\sqrt{8\ln 2}\lambda_0)$ would be introduced, where $\phi_0$ represents the phase shift at center wavelength. The swept source provides the advantage of controlling the phase shift during wavelength sweeping. In our system, drive signals of the polarization modulator were carefully calibrated according to the swept spectra function to obtain a constant phase shift across the total spectrum. With $\lambda_0$ = 1310 nm and $\Delta\lambda$ = 85 nm, a 2.8% or 2.5° average polychromatic phase error was corrected for the phase shift of $\pi/2$. The phase correction for the current system is not significant because of the limited source bandwidth used. However, in the case of a high resolution system with a broadband light source, the polychromatic phase error cannot be neglected and this correction will be essential for accurate quantification of polarization properties of biological tissues.

#5440 - $15.00 US Received 7 October 2004; revised 19 November 2004; accepted 19 November 2004

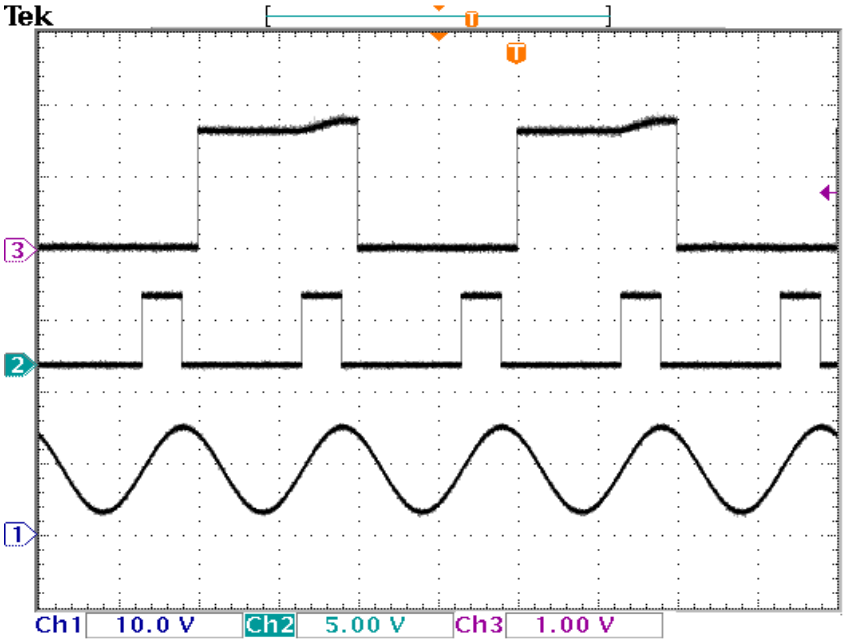


Fig. 2. Synchronizing time clock diagram for the FDOCT system. Channel 1 is the sinusoidal signal to drive the swept source. Channel 2 is the signal used to trigger data acquisition. Channel 3 is the drive signal to control the polarization modulator.

The complex analytical depth encoded signal $\tilde{S}(z)$ was converted from the time fringe signal $\Gamma(t)$ by the digital approach shown in the following block diagram:

$$\Gamma(t) \rightarrow \boxed{FFT} \rightarrow \boxed{\times H(v)} \rightarrow \boxed{\text{Bandpass Filter}} \rightarrow \boxed{\text{Demodulation}} \rightarrow \boxed{FFT^{-1}}$$

$$\rightarrow \tilde{\Gamma}(t) \rightarrow \boxed{\text{Spectra Calibration}} \rightarrow \tilde{I}(k) \rightarrow \boxed{FFT} \rightarrow \tilde{S}(z)$$

where FFT denotes the fast Fourier transform, $\times$ is a multiplying symbol, $H(\nu)$ is the Heaviside function given by:

$$H(v) = \begin{cases} 0 & v < 0 \\ 1 & v \geq 0 \end{cases} \tag{1}$$

and FFT$^{-1}$ denotes the inverse fast Fourier transform. The time fringe signal $\Gamma(t)$ is first transformed from time to frequency space by FFT. Multiplication of $H(\nu)$ selects the positive term of the Fourier transformed signal. The signal is then bandpass filtered with a 400 kHz bandwidth filter to remove the low frequency and DC noises. The subsequent demodulation step shifts the center frequency of the filtered interference term from 1 MHz to zero. The frequency fringe signal is then converted back to time space by inverse FFT. To cancel the distortion originating from the nonlinearities in the wavenumber function $k(t)$, the data was numerically remapped from uniform time to uniform wavenumber space based on the function of $k(t)$ which is determined by the spectra calibration process described previously. The last FFT performed in $k$ space retrieved the complex depth encoded fringe signal

#5440 - $15.00 US Received 7 October 2004; revised 19 November 2004; accepted 19 November 2004

$\tilde{S}(z) = A(z)e^{i\phi(z)}$ which contains both the amplitude $A(z)$ and phase $\phi(z)$ terms. The measured sensitivity enhancement is about 20 dB after cancellation of the autocorrelation and DC noises. The imaging range was doubled from 2 mm to 4 mm with removal of the mirror image.

From the complex signals of the two orthogonal channels, the Stokes vector for the axial pixel z and one polarization state can be calculated as:

$$\begin{aligned} I(z) &= \tilde{S}_H(z)\tilde{S}_H^*(z) + \tilde{S}_V(z)\tilde{S}_V^*(z) \\ Q(z) &= \tilde{S}_H(z)\tilde{S}_H^*(z) - \tilde{S}_V(z)\tilde{S}_V^*(z) \\ U(z) &= 2\,\mathrm{Re}\left[\tilde{S}_H^*(z)\tilde{S}_V(z)\right] \\ V(z) &= 2\,\mathrm{Im}\left[\tilde{S}_H^*(z)\tilde{S}_V(z)\right] \end{aligned} \tag{2}$$

where I, Q, U and V are the four components of the Stokes vector. $\tilde{S}_H(z)$ and $\tilde{S}_V(z)$ are the complex signals from the horizontal and vertical polarization channels at axial pixel z, respectively, $\tilde{S}_H^*(z)$ and $\tilde{S}_V^*(z)$ are their conjugates, respectively. From the Stokes vectors for the two polarization states, the polarization diversity intensity image was obtained by averaging the two I. To determine the birefringence image, the detected signal reflected from the surface of the sample was adopted as the reference. The phase retardation was calculated by comparing the Stokes vectors between the surface and deeper axial position [10].

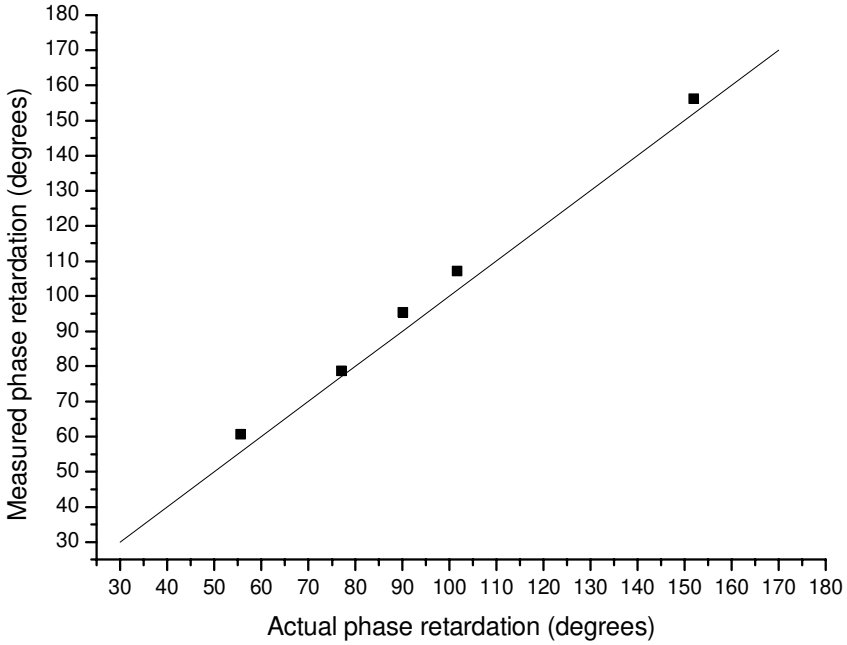


Fig. 3. Measured phase retardation versus actual phase retardation for different wave plates. The round-trip retardation values of the wave plates for measurement are 55.5°, 77°, 90°, 101.6° and 151.9°, respectively. The solid line represents the actual phase retardation and the points represent the measured phase retardation.

#5440 - $15.00 US Received 7 October 2004; revised 19 November 2004; accepted 19 November 2004

## 3. Experimental results

To evaluate the system and processing method, standard wave plates with different retardation (Casix, Inc.) were used as samples. The retardation values of these wave plates were previously calibrated using a polarimeter (Thorlabs). For each wave plate, 200 A scans were averaged to determine the phase retardation values which are presented in Fig. 3. The average error of the measured phase retardation compared with calibrated values was 4.5° and the average standard deviation was 4.1° which demonstrates that the experimental data are in good agreement with expected theoretical values. The measured result is similar to those reported with TDOCT systems [11-12].

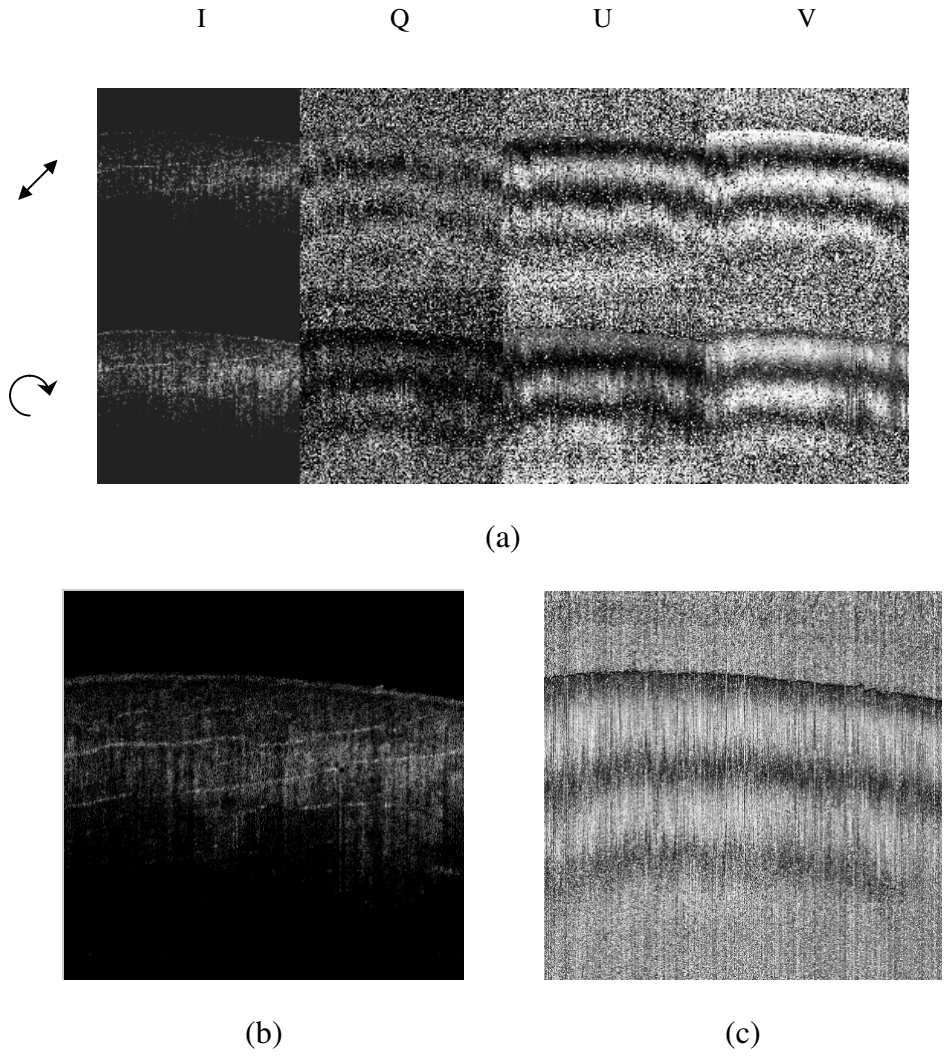


Fig. 4. Images of the Stokes vectors, polarization diversity intensity and phase retardation in rabbit tendon. (a): Stokes vector images corresponding to the two input polarization states; (b): polarization diversity intensity image; and (c): phase retardation image.

#5440 - $15.00 US Received 7 October 2004; revised 19 November 2004; accepted 19 November 2004

To illustrate the performance of the system in biological tissues, rabbit tendon was imaged. The simultaneous imaging of the Stokes vectors, polarization diversity intensity and birefringence is shown in Fig 4. The imaged area is 4 × 3.9 mm with the zero distance difference set in the center of the depth scale. The top four panels (Fig.4a) are the Stokes vectors corresponding to the two different polarization states. The bottom panel images are polarization diversity intensity (Fig.4b) and phase retardation (Fig.4c) images.

## 4. Summary

In summary, a fiber based polarization-sensitive FDOCT system was demonstrated. The Stokes vectors, polarization diversity intensity and birefringence images in biological tissue were obtained by processing the analytical complex fringe signals from two polarization channels.

## Acknowledgments

This work was supported by research grants from the National Science Foundation (BES-86924), National Institutes of Health (EB-00293 and EB-002495, NCI-91717, RR-01192), Air Force Office of Scientific Research (FA9550-04-1-0101), and the Beckman Laser Institute Endowment. Loan of the 1.31 μm swept source from Micron Optics, Inc. and discussions with Kevin Hsu are also gratefully acknowledged.

#5440 - $15.00 US Received 7 October 2004; revised 19 November 2004; accepted 19 November 2004